13th IEA Heat Pump Conference
April 26-29, 2021 Jeju, Korea

Evaluation of a Hybrid AC/DC Powered Residential Split-System Heat Pump Performance using a DC Nanogrid

Jonathan Ore[a,*], Fatih Meral[a], Oliver Obst[a], Orkan Kurtulus[a], Eckhard A. Groll[a]

[a]Purdue University, Ray W. Herrick Laboratories 177 S. Russell St., West Lafayette 47907, USA

Abstract

Many benefits have been observed from the employment of Direct Current (DC) distribution schemes over those of traditional Alternating Current (AC) within building architectures, ranging from enhanced system efficiency, increased reliability, reduced points of failure, and more convenient integration with renewable energy generation systems. The objective of this research is to demonstrate the emulation of a DC Nanogrid system supporting the largest categorical energy consumer in the residential building-space: the HVAC system. Through the avoidance of unnecessary energy losses due to power conversion, a DC-driven heat pump affords a significant opportunity for energy savings and overall improved efficiency. This paper presents the results from laboratory testing a hybrid AC/DC powered air-source heat pump fashioned to operate separately on either an AC or DC electrical supply. The corresponding residential DC Nanogrid system is simulated with a psychrometric chamber integrating a variable voltage DC power supply. Initial psychrometric testing of both AC and DC configurations are presented, along with corresponding thermal and electrical performance analysis. Future work will consider individual characterization of the heat pump components under DC supply, comparison of line losses between AC and DC load conditions, and additional environmental heating and cooling test cases.

Keywords: DC Power; Direct Current; Nanogrid; Heat Pump

1. Introduction

Within the U.S., the advent of ever-increasing energy demands has resulted in escalating strain on the power grid, often pressuring it to the limits of its capabilities. Modern technological innovations have fostered a greater dependency on the grid, coupling it with nearly every aspect of contemporary society. Unfortunately, the grid has not experienced a parallel rate of growth alongside technology, with some estimates reporting in the range of trillions of dollars necessary for repairs and upgrades to return to a nominal performance level. During the previous decade, the American Society of Civil Engineers scored the U.S. energy system with a grade of a "D+" for overall reliability, describing outdated distribution systems, limited system capacity, and undesirable environmental side-effects as the leading factors in their evaluation [1]. Further challenging these conditions is the increasing dependency on internet technology and cellular networks, resulting in a proportional rise in vulnerability of the electrical grid. A recent Wall Street Journal article concludes that a failure of just nine substations (via targeted attack, electrical failure, etc.) could result in a significant destabilization of the entire electrical grid [2].

These concerns have stimulated investigations into other potential solutions, including the feasibility of individual micro and nanogrids existing in both residential and commercial spaces. These grids, while still connected to the outside "main" electrical grid, possess the ability to operate autonomously and mitigate loads in an islanding-mode without relying on the external grid. Such capabilities are highly beneficial in the face of emergencies or other failures, but also offer advantages in energy costs through the employment of renewable energy sources (e.g. wind, solar, geothermal, etc.). The electrical infrastructure afforded by a micro/nanogrid is typically that of Direct Current (DC), as opposed to the traditional infrastructure of Alternating Current (AC)

* Corresponding author. Tel.: +1-765-494-2132.
E-mail address: jore@purdue.edu.

currently in place. Unfortunately, nearly all appliances and devices, particularly in a residential setting, require DC power at terminal endpoints; as a result, the AC power being supplied to them must first be converted to DC, resulting in a loss of energy. This problem is further exacerbated when renewable energy is integrated, which naturally generates DC power. To provide compatibility with the existing infrastructure, energy generated from renewable resources must first undergo a conversion from DC to AC, resulting in energy loss, and then experience a second conversion from AC back to DC at the point of use, resulting in additional energy loss. Such penalties are primary drivers for interest in a DC-based micro/nanogrid solution, with some modeling estimations revealing a potential conversion loss reduction of up to 30% in a commercial building with an integrated battery [3].

The residential setting in this paper serves as the foundation for a novel type of nanogrid, which seeks to achieve a complete home conversion from AC to DC power. Nanogrid terminology is employed to differentiate the intra-building scope of the design, as opposed to a microgrid which often encapsulates multiple buildings and distributed energy generation sites and storage. The dwelling under scrutiny is a two-story 1920's era home entitled "The DC House", housing three graduate students and located in West Lafayette, IN. The DC House is situated on a 595 m^2 lot with a detached garage, and contains 208 m^2 of floor space. As part of the conversion process from AC to DC, a DC infrastructure will be designed and installed, and supplied by renewable energy sources using solar panels on the roof of the house. Modeling and simulation are planned to verify and validate the hardware solution, as has been performed in similar setups [4].

With the house serving as a "living lab", baseline AC energy consumption among the residents was evaluated for an entire year. Analysis of data collected during 2018 revealed the heat pump system to be the largest categorical energy consumer of all appliances present.

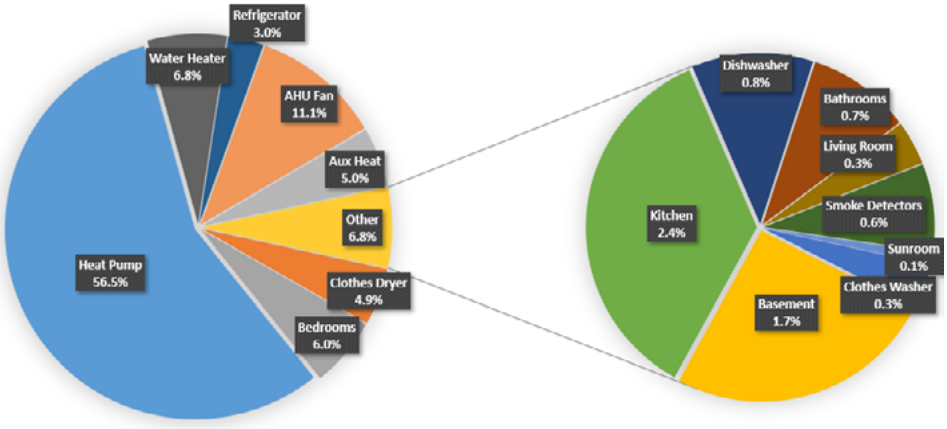

Fig. 1. DC House Categorical Comparison of Appliance Energy Consumption in 2018

A survey performed by the IEA confirms the findings in Fig. 1, estimating that space heating and air conditioning represent up to 49% of average U.S. household energy consumption [5]. As a result, electrical retrofitting of the heat pump from an AC to DC configuration affords a significant opportunity for energy savings and an increase in efficiency.

In this paper, the DC Nanogrid is simulated through the use of a variable-voltage 15 kW DC power supply. The environmental conditions inside and outside the DC House are emulated using two adjacent psychrometric chambers, capable of replicating conditions between -20 °C (-4 °F) and 55 °C (130 °F), and 15% to 100% humidity. AC and DC electrical configurations using a retrofitted hybrid heat pump are tested under a variety of cooling conditions, and compared with thermal and electrical performance metrics. Further testing conditions and topics of investigations are then considered for future study.

2. Specifications and Methods

To provide a basis for comparison across the various electrical configurations, an off-the-shelf variable speed heat pump with scroll compressor was selected and retrofitted to accept both AC and DC electrical

supply inputs. Using conventional residential AC power, the modified unit operates on a nominal split-phase 240 VAC input. Under the DC configuration, the modified unit operates on nominal bi-polar 350 VDC input, with undervoltage and overvoltage limits at 250 VDC and 400 VDC, respectively. The internal thermal configuration in the modified unit remained unchanged in order to ensure commonality. The results within this paper evaluate thermal and electrical performance with both AC and DC power conditions using the retrofitted AC/DC hybrid unit. Future investigation will then consider this data against an unmodified unit installed at the DC House operating on standard 240 VAC.

2.1. Electrical Configuration and Conversion Losses

A specific advantage of the DC-based electrical configuration arises from the difference in current consumption of the heat pump. The maximum power of the heat pump is rated at 6.96 kW, which can be used to determine the maximum current load under a 120 VAC split-phase configuration.

$$P_{AC} = I_{AC} \cdot \Delta V_{AC} \quad (1)$$

Under this relationship, the maximum current is found to be approximately 29 A. If the voltage is then increased to 350 VDC for the DC connection, the maximum current is proportionally decreased to 20 A instead. Eq. 1 can be rewritten to describe the loss of power with respect to the line resistance, as is shown in Eq. 2.

$$P_{Loss} = I^2 \cdot R \quad (2)$$

From this relationship, it is clear that the loss of power associated with resistance in the system is reduced in proportion to the squared inverse of current. As a result, halving the current requirement for a component could potentially reduce its electrical line transmission power losses by a factor of one-fourth. In the specific case of the heat pump under study in this paper, the decrease in current requirements from 29 A to 20 A affords a theoretical maximum reduction in line power loss of up to 52%, assuming equivalent resistances.

Although the line power consumption represents only a small portion of the energy consumed by the heat pump system, the savings become more significant over larger distances and across numerous appliances. These losses also reduce result in a voltage drop between supply and appliance, potentially reducing performance and introducing system instability. Additional current requirements also impose an increase in the wire gauge, resulting in higher costs and even further possible line losses. These factors will be closely analyzed in future studies to numerically quantify differences between AC and DC configurations, and their corresponding transmission losses under a variety of line lengths.

In a traditional electrical design, input three-phase AC voltage is passed through a bridge rectifier, converting it to a usable DC voltage as shown in Fig. 2.

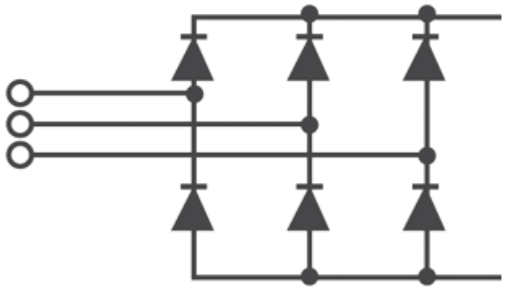

Fig. 2. Standard Three-Phase Bridge Rectifier Circuit

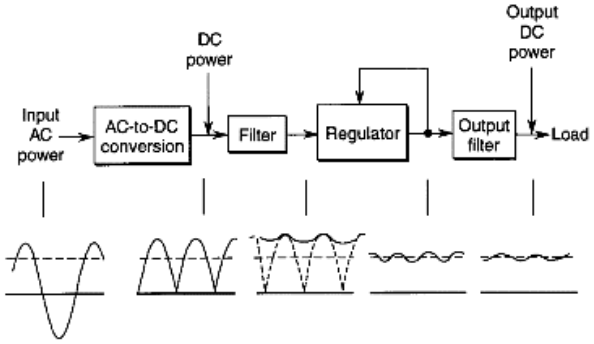

Fig. 3. Complete Power Conversion Process from AC to DC [6]

The entire conversion process can be summarized using the flow diagram in Fig. 3, with the corresponding electrical waveform shown immediately underneath. The rectification stage in Fig. 2 is represented in Fig. 3 by the "AC-to-DC conversion" block. As Fig. 3 illustrates, this first stage of rectification results in the largest source of energy lost. Through the ratcheting-effect of the diodes in the rectifier, the negative phase of the AC waveform is removed in the first step towards the DC conversion. The collective result of each stage in Fig. 3 can yield a net loss of 10% to 15% or more in energy efficiency.

The internal control mechanisms of the modified heat pump have been designed to accept both conventional AC voltage and DC input. The hybrid nature of the modified heat pump is made feasible in part by the capability of the bridge rectifier in Fig. 2 to allow DC voltage to pass through without significant impedance. In the case of a pure DC voltage, which is constant without any sinusoidal component, the diodes have no impact on the path of current outside of a small voltage drop, and therefore do not inhibit the processing of the DC input. The remaining conversion stages (filter, regulator, etc.) also have no significant impact on an input DC voltage, and thus the final output DC power shown in Fig. 3 is still achieved.

2.2. Hybrid Heat Pump Setup and Specifications

Initial experimental data for the hybrid heat pump was collected using a 230 VAC connection available within the psychrometric chambers. Within the U.S., 220 VAC to 240 VAC are generally understood as synonymous, and thus the DC House and psychrometric laboratory setting can be considered electrically equivalent for future studies. The hybrid heat pump under study is a 14.07 kW (4 ton) air-source split-system design, accepting either 240 VAC or 350 VDC as inputs. Indoor and outdoor components of the heat pump were installed separately in individual psychrometric chambers to properly emulate realistic environmental conditions at the DC House. The outdoor unit contains a compressor, condenser, outdoor fan, and a four-way valve, while the indoor unit includes the evaporator, thermostatic expansion valve (TXV), and indoor fan. The heat pump unit contains a scroll compressor, and a manufacturer Seasonal Energy Efficiency Ratio (SEER) value of 18. The nominal indoor airflow rate is 2379 m^3/h, and the hybrid system is charged with 6.1 kg of R410A. The heat pump system is composed of a variable speed compressor, an indoor fan with variable volume flow rate, and an outdoor fan with a variable speed motor. The specifications are summarized in Table 1.

Table 1. Hybrid Heat Pump Configuration Summary

Available electrical configurations	Cooling capacity	SEER rating	Refrigerant	Testing environment
240 VAC / 350 VDC	14.07 kW (4 ton)	18	R410A	Psychrometric Chambers

2.3. Equipment Setup and Data Collection

Laboratory data from the hybrid heat pump was collected using a National Instruments cRIO-2091 data acquisition system (DAQ) with a LabVIEW based visual interface for inspection and logging. Watt transducers were individually installed to monitor the AC power consumption of the indoor unit fan, and the outdoor unit fan and compressor. When employing the DC power configuration, cumulative system power was monitored

using the 15 kW MagnaPower variable-voltage DC power supply. DC power was distributed to the indoor unit using 20 m of 10 AWG wire, and to the outdoor unit using 10 m of 6 AWG wire.

Thermal data collected was evaluated using both air and refrigerant enthalpy methods to determine the cooling capacity. A schematic summarizing the psychrometric chamber layout and refrigeration loop configuration is provided in Fig. 4, with the state point descriptions given in Table 2.

Table 2. Hybrid Heat Pump State Point Definitions

State Point	Description
1	Compressor Inlet
2	Compressor Outlet
3	Condenser Inlet
4	Condenser Outlet
5	EXV Inlet
6	EXV Outlet
7	Evaporator Inlet
8	Evaporator Outlet

Thermophysical properties from the psychrometric test setup were determined through the use of the Engineering Equation Solver (EES) software [7]. In addition, state points 1 through 5 and 7 in Fig. 4 could be calculated from the measured pressure and temperature values of the refrigerant. State point 6 between TXV and the evaporator was obtained assuming both an isenthalpic expansion across the TXV device and negligible pressure drop at the outlet of the TXV and evaporator. The refrigerant mass flow was determined using a Coriolis mass flow meter configured for liquid phase between state points 4 and 5.

Cooling capacity of the hybrid heat pump could be calculated through two separate means, and then compared to determine the accuracy of the system measurements. Using a First Law energy balance and the given assumptions at each state point, the evaporator cooling capacity can be computed from Eq. 3.

$$\dot{Q}_{evap} = \dot{m}\Delta h_{evap} = \dot{m}(h_7 - h_6) \tag{3}$$

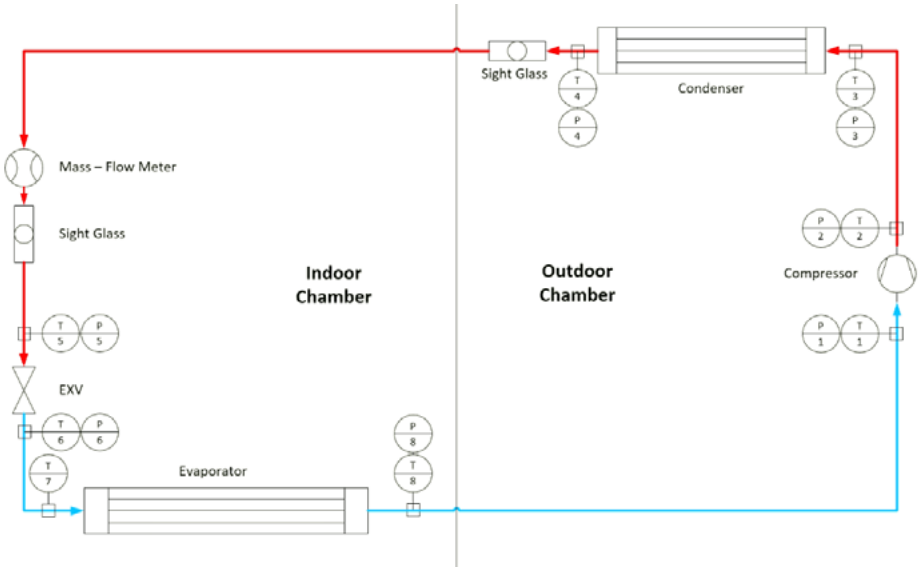

Fig. 4. Hybrid Heat Pump Cooling Configuration Schematic – Psychrometric Chamber Setup

The net capacity is then calculated by taking the difference between the cooling capacity of the evaporator from Eq. 3, and the additional heat added to the system from the indoor fan. The amount of heat was assumed approximately equivalent to the overall power consumption of the indoor unit, resulting in the relationship given by Eq. 4.

$$\dot{Q}_{delivered} = \dot{Q}_{evap} - \dot{W}_{indoor} \tag{4}$$

Alternatively, the hybrid heat pump cooling capacity could also be determined using an air-side approach. In this evaluation, the overall air-side capacity can be calculated again by considering a First Law energy balance applied to the indoor unit. Within this energy balance, the difference in enthalpy of the air flow is accounted for, along with the phase change of water condensed within the unit, yielding Eq. 5.

$$\dot{Q}_{delivered} = \dot{m}_{air}\Delta h_{evap} - \dot{m}_{water}h_{water} \tag{5}$$

In order to evaluate Eq. 5, calculation of the mass of air flow is needed. This can be determined by analyzing the volume flow rate of the nozzle box in line with the indoor unit's duct work of the indoor unit, which is designed in compliance with ASHRAE Standard 37-2009 [8]. The volumetric flow rate is calculated iteratively using Eq. 6.

$$\dot{V}_{air} = Y\sqrt{\frac{2\Delta p_{nozzle}}{\rho_{air}}}\sum_{0}^{k} C_i A_i \tag{6}$$

The expansion factor (Y) and coefficient of discharge (C_i) in Eq. 4 are defined in ASHRAE Standard 37-2009, and the area of the duct work (A_i) was specified during system installation [8]. With the volumetric flow rate obtained, the air flow mass can be solved by multiplying by the air density, and illustrated in Eq. 7.

$$\dot{m}_{air} = \dot{V}_{air}\rho_{air} \tag{7}$$

In addition to the mass of the air flow, the mass of the condensed water flow is also needed to evaluate Eq. 5. EES is used to calculate the inlet air enthalpy, outlet water enthalpy, and outlet air enthalpy, provided the necessary inputs are given. This includes the air dry-bulb temperature, which is measured with a 3x3 thermocouple grid situated between the inlet and outlet of the indoor unit, the relative humidity of inlet air using a relative humidity sensor, and the dew point of the outlet air. The dew point is determined through a periodic sampling of the air at the rate of 1 L/min, which is then processed through a chilled mirror dew point sensor. The relationship between these values calculated in EES is detailed in Eq. 8.

$$\dot{m}_{water} = \dot{m}_{air}(\omega_2 - \omega_1) \tag{8}$$

Finally, the heat pump coefficient of performance (COP) can be tabulated by dividing the system cooling capacity by its power consumption, as defined in Eq. 9.

$$\mathrm{COP} = \frac{\dot{Q}_{delivered}}{\dot{W}_{total}} \tag{9}$$

2.4. Testing Methodology

The hybrid heat pump with variable-speed components was tested in accordance with the guidelines set by AHRI. To establish common baseline testing conditions for both the AC and DC electrical configurations, psychrometric indoor and outdoor room conditions were specified from test conditions A, B, C, D, and E from Table 8 of the AHRI Standard 210/240 [9]. The compressor was operated near full speed during each test, but not explicitly controlled under either AC or DC configuration.

The test conditions performed are collected into a matrix shown in Table 3, with temperature values provided in both English and SI Units because SEER calculations require the input of temperatures in °F. Each test case was performed under both the 230 VAC and 350 DC configuration under steady state conditions, and monitored for thermal and electrical characteristics every few seconds. This data was subsequently post-processed using the EES software at the conclusion of the testing.

Table 3. Hybrid Heat Pump Psychrometric-Based Test Matrix

Test Case	Cycle Configuration	Indoor Temperature [°F/°C]	Indoor Relative Humidity [%]	Outdoor Temperature [°F/°C]	Indoor Relative Humidity [%]
1	Cooling	80/26.7	51.10	95/35	39.60
2	Cooling	80/26.7	51.10	82/27.8	39.90
3	Cooling	80/26.7	51.10	87/30.6	40.20
4	Cooling	80/26.7	51.10	82/27.8	39.90
5	Cooling	80/26.7	51.10	67/19.4	40.30

2.5. COP and EER Analysis

The test matrix described in Table *3*. Hybrid Heat Pump Psychrometric-Based Test MatrixTable 3 is also leveraged to evaluate the COP and the Energy Efficiency Ratio (EER) ratings for the hybrid heat pump system. These ratings, along with the SEER calculation, are standard methods used to rate the heating and cooling performance of U.S. heat pumps. A seasonal analysis is necessary to characterize the benefits of a variable speed system, which come in form of the ability to match part-load conditions. The COP and EER ratings are used in this study to quantify the thermal performance of each test case under the AC and DC configurations of the hybrid heat pump.

3. Results

The results of the hybrid heat pump testing under the AC and DC electrical configurations of the test matrix in Table 3 are detailed in Table 4 and Table 5.

Table 4. Hybrid Heat Pump 230 VAC Test Results

Test Case	Electrical Configuration [VAC]	Cooling Capacity [kW]	Indoor Power [kW]	Outdoor Power [kW]	Total Power [kW]	COP [-]	EER [-]
1-AC	230	12.8	0.4478	3.6204	4.0682	3.15	10.8
2-AC	230	14	0.4515	3.1088	3.5603	3.93	13.4
3-AC	230	13.6	0.3357	3.2627	3.5984	3.78	12.9
4-AC	230	14.1	0.3238	3.0835	3.4073	4.14	14.1
5-AC	230	15.4	0.3568	2.5475	2.9043	5.30	18.1

Table 5. Hybrid Heat Pump 350 VDC Test Results

Test Case	Electrical Configuration [VDC]	Cooling Capacity [kW]	Total Power [kW]	COP [-]	EER [-]
1-DC	350	13.3	3.9050	3.38	11.3
2-DC	350	14.1	3.3260	4.24	14.1
3-DC	350	13.9	3.4557	4.02	13.9
4-DC	350	14.3	3.2429	4.41	14.3
5-DC	350	15.8	2.8138	5.62	15.8

The cooling capacity, COP, and EER measured in each of the test cases was acquired using the refrigerant method calculation. Although these capacities were similar in magnitude between AC and DC configurations, the thermal state points of the refrigeration cycle maintained some significant differences, especially at the compressor suction temperature. To consider these more closely, the thermal characteristics of the first test case under both the AC and DC configurations are presented in Table 6.

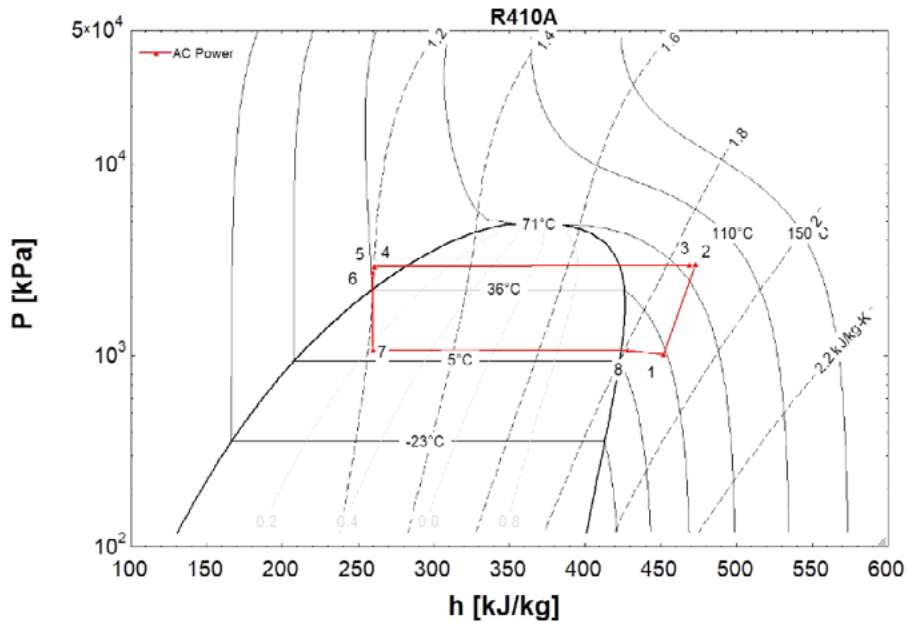

Table 6. Hybrid Heat Pump Test Case 1 Thermal Characteristics

Test Case	Electrical Configuration [-]	Indoor Air Flow [m^3/s]	Compressor Suction Superheat [C]	Compressor Suction Temperature [C]	Compressor Suction Pressure [kPa]	Compressor Discharge Temperature [C]	Compressor Discharge Pressure [kPa]
1-AC	230 VAC	0.6269	24.6	33.9	1016	81.2	3003
1-DC	350 VDC	0.6892	6.1	15.0	997.6	81.6	3002

As Table 6 reveals, the DC configuration maintained a higher indoor air flow rate under steady state conditions and a significantly lower compressor suction temperature. The state points for the AC and DC configurations under test case 1 are further illustrated in the P-h diagram shown in Fig. 5 and Fig. 6.

Since the compressor speed was controlled automatically by the heat pump, this may have resulted in the differences observed. In addition, the drive operation under DC conditions could not be readily evaluated against those under the AC configuration without supplemental manufacturer data. As a result, these factors demonstrated a need for further instrumentation and analysis to determine the source of the differences. Additional DC-watt transducers are planned for installation on the indoor and outdoor unit for increased fidelity of the power consumption, as well as coordination with service data to extract the compressor speeds in post-processing.

Fig. 5. P-h Diagram for the AC Configuration Running Test Case 1

3.1. DC Measurement Uncertainty Analysis

The DC power supply served as both the representative DC Nanogrid supply for the hybrid heat pump, and the monitoring device to capture the heat pump total power consumption. As a result of the significant dependence on this unit, uncertainty of the supply and monitoring capabilities is considered. From the supply side, the manufacturer specifications indicate an output load regulation of ±0.01% of full-scale voltage under a voltage control mode. In addition, an input line regulation of ±0.004% of full-scale voltage is maintained under the same voltage control. Load regulation in this case refers to the capacity of the power supply to maintain a specified output voltage while the load is varying, and line regulation describes the ability of the power supply to maintain the same specified output voltage while the input supply power to the power supply is varying. Collectively, these represent a combined uncertainty of ±0.011%. This is calculated using a

quadratic sum, which describes the uncertainty in measurements x, …, y, which are used to compute an uncertain output, δf. This is given below in Eq. 10.

$$\delta f = \sqrt{(\delta x)^2 + \cdots + (\delta z)^2} \tag{10}$$

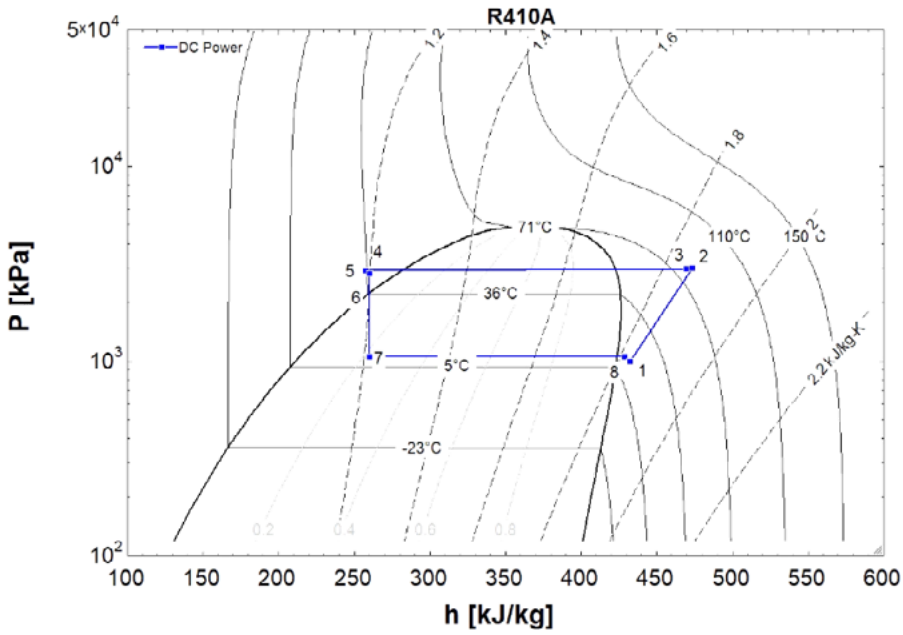

Fig. 6. P-h Diagram for the DC Configuration Running Test Case 1

Defining the full-scale voltage of the power supply to be 500 VDC, the output supply to the heat pump is calculated with an uncertainty of 0.054 VDC. These results are summarized in **오류! 책갈피가 자신을 참조하고 있습니다.**, where $\Delta V_{Controlled}$ represents the 350 VDC measured operating condition.

Table 7. DC Power Supply Output Uncertainty

Uncertainty Condition	Uncertainty [%]	Voltage Error [VDC]
Line Regulation	0.01	$V_{controlled} \pm 0.05$
Load Regulation	0.004	$V_{controlled} \pm 0.02$
Output Supply	0.011	$V_{controlled} \pm 0.054$

Using the power supply to monitor the heat pump power consumption, the measurement accuracy must then be considered. The manufacturer specifies a voltage readback uncertainty of ±0.2% of full-scale voltage, and a current readback uncertainty of ±0.02% of full-scale current. Defining the full-scale current of the power supply to be 30 A, the cumulative power measurement uncertainty reading can be tabulated as shown in Table 8. Since the power is calculated by the multiplication of the DC voltage and current, the resulting uncertainty is defined as the quadratic sum multiplied by the power measurement.

Table 8. DC Power Supply Measurement Uncertainty

Uncertainty Condition	Uncertainty [%]	Error
Voltage Reading	0.02	$V_{measured} \pm 0.1$ [V]
Current Reading	0.02	$I_{measured} \pm 0.006$ [A]
Power Measurement	0.011	$P_{measured} \pm 0.100$ [W]

4. Conclusions and Future Studies

This research presented the psychrometric evaluation of a retrofitted hybrid heat pump unit under a variety of environmental conditions using both AC and DC electrical configurations. The intent of this research is to demonstrate the feasibility of DC retrofits of devices traditionally configured for AC inputs, and to analyze improvements in performance and energy efficiency through the avoidance of AC and DC conversions. The DC power was supplied using a variable voltage power supply, which was implemented to represent a DC Nanogrid operating in a residential setting. The unit functioned successfully using a 350 VDC input, and was able to perform under each of the five test conditions described in Table 3. Based on the thermal and electrical measurements obtained, a need for additional instrumentation and further testing was identified. DC-based watt transducers are planned for installation on the indoor and outdoor units to provide insight into their representative energy consumption. This data coupled with supporting manufacturer measurements will be used to both verify the results obtained within this paper and analyze the difference in behavior between the AC and DC modes of operation. These results, along with additional test conditions and repeated trials, will be provided in a follow-on paper.

Beyond the laboratory setting, additional studies will analyze the hybrid heat pump results described here against an unmodified heat pump unit installed in the DC House using load-based testing methodology. These subsequent investigations will assist in confirming the hybrid heat pump AC and DC data obtained in this paper, and further support the potential energy improvement opportunities under DC operation. In addition, coordinated testing between the hybrid heat pump and unmodified heat pump is planned in order to establish a proportional relationship between testing results. Under this methodology, ambient temperature and humidity from the residential testing environment will be relayed in real-time to the test setup in the psychrometric chambers, allowing it to be recreated and applied to the heat pump under scrutiny there. These test results will be described in a future paper.

Nomenclature

Variable	Description	Units
A	Area	m^3
C	Coefficient of discharge	-
h	Specific enthalpy	kJ/kg
$\dot{m}$	Mass flow	kg/s
p	Pressure	kPa
$\dot{Q}$	Cooling capacity	W
T	Temperature	K
$\dot{V}$	Volume air flow	m^3/s
$\dot{W}$	Power	W
Y	Expansion factor	-

Greek Symbol	Description	Units
ρ	Area	m^3
ω	Coefficient of discharge	-
δ	Uncertainty	-

Acronyms

AC	Alternating Current
AHRI	Air-Conditioning, Heating, and Refrigeration Institute
COP	Coefficient of Performance
DAQ	Data Acquisition System
DC	Direct Current
EER	Energy Efficiency Ratio
EES	Engineering Equation Solver
EXV	Electronic Expansion Valve
HVAC	Heating, Ventilation and Air Conditioning
LabVIEW	Laboratory Virtual Instrumentation Engineering Workbench
RPM	Rotations Per Minute
SEER	Seasonal Energy Efficiency Rating
US	United States
VAC	Voltage AC
VDC	Voltage DC

Subscripts

1, 2, 3, …	State Points
air	Air
controlled	Controlled Quantity
delivered	Net capacity
evap	Evaporator
indoor	Indoor
measured	Measured Quantity
nozzle	Nozzle Box
total	Total
water	Water

Acknowledgements

The authors would like to thank the Center for High Performance Buildings (CHPB) at the Ray W. Herrick Laboratories, Purdue University for the financial support of this study. In addition, the authors express their sincere gratitude to Parveen Dhillon and Rob Hughes for their excellent assistance in testing and troubleshooting equipment.

References

[1] Lacey S. 2013. America Gets a D in Energy Infrastructure, *Greentech Media*.
[2] Tweed K. 2014. Attack on Nine Substations Could Take Down U.S. Grid, *IEEE Spectrum*.
[3] Hofer J, Svetozarevic B, Schlueter A. 2017. Hybrid AC/DC building microgrid for solar PV and battery storage integration, *IEEE Second International Conference on DC Microgrids*. 2:188-191
[4] Jie LR, Naayagi RT. 2019. Nanogrid for Energy Aware Buildings. *IEEE PES GTD Grand International Conference and Exposition Asia.* 92-96.
[5] Baxter V, Sikes K, Domitrovic R., Amrane K. 2014. IEA HPP Annex 42: Heat Pumps in Smart Grids. Task 1: Market Overview. ORNL/TM-2014/73.
[6] Fowler K. 2000. Power Supply Design and Distribution. *IEEE Instrumentation and Measurement.* 3(4):42-46.
[7] Klein S. 2018. "Engineering Equation Solver", F-Chart Software, v.10.268.
[8] ASHRAE Standard 37. 2009. Methods of Testing for Rating Electrically Driven Unitary Air-Conditioning and Heat Pump Equipment, *ASHRAE Standard*.
[9] AHRI Standard 210/240. 2017. Performance Rating of Unitary Air-conditioning & Air-source Heat Pump Equipment, *AHRI Standard*.